Critical behavior and magnetocaloric effect of the quasi-two-dimensional room-temperature ferromagnet Cr$_4$Te$_5$

Luo-Zhao Zhang,[1] An-Lei Zhang,[1] Xiu-De He,[1] Xin-Wei Ben [©],[1] Qi-Ling Xiao,[1] Wen-Lai Lu,[1]
Fei Chen,[1] Zhenjie Feng,[1] Shixun Cao [©],[1,2] Jincang Zhang,[1] and Jun-Yi Ge [©][1,3,*]

[1]*Materials Genome Institute, Shanghai University, 200444 Shanghai, China*
[2]*Department of Physics, Shanghai University, 200444 Shanghai, China*
[3]*Shanghai Key Laboratory for High Temperature Superconductors, Shanghai University, 200444 Shanghai, China*

A high-quality Cr$_4$Te$_5$ single crystal was prepared by the chemical vapor transport method. The crystal structure, magnetic properties, and magnetocaloric effect have been investigated in detail. Its critical behavior was methodically studied by measuring isothermal magnetization curves around the ferromagnetic to paramagnetic phase transition temperature. The critical exponents $\beta = 0.388$, $\gamma = 1.29$, $\delta = 3.93$, and Curie temperature $T_C = 318.7$ K were determined with modified Arrott plots, the Kouvel-Fisher method, critical isotherm analysis, and wisdom scaling law, respectively. The obtained critical exponents were self-consistent and follow the scaling equation around T_C, indicating the reliability of these values. Further analysis revealed that the spin coupling inside Cr$_4$Te$_5$ exhibits three-dimensional Heisenberg-like behavior with long-range magnetic interaction and that the exchange interaction decays as $J(r) \approx r^{-4.85}$.

I. INTRODUCTION

The discovery of two-dimensional (2D) materials such as graphene [1] has ignited a research boom due to their tunable electronic properties and tremendous potential applications in spintronic devices [2–4]. Among all the 2D materials, extensive investigations have been devoted for the purpose of clarifying the nature of ferromagnets down to the monolayer. Layered ferromagnets such as Cr$_2$Ge$_2$Te$_6$ [5,6], Cr$_2$Si$_2$Te$_6$ [7], Fe$_3$GeTe$_2$ [8], and CrI$_3$ [9–11] have attracted great attention, since long-range ferromagnetism persists in a few layers. Theoretically, according to the Mermin-Wagner theorem [12], spontaneous magnetization does not exist in the 2D isotropic Heisenberg model at a finite temperature. However, magnetocrystalline anisotropy lifted this restriction, making it possible to obtain a 2D Ising ferromagnet [13]. Therefore, magnetocrystalline anisotropy is the key point to realize two-dimensional ferromagnetic materials. Even though long-range magnetism in monolayers has been achieved, the Curie temperature is much lower than RT, e.g., 61 K for CrI$_3$, 61 K for Cr$_2$Ge$_2$Te$_6$, 32 K for Cr$_2$Si$_2$Te$_6$, thus limiting their spintronic applications. Numerous approaches have been applied to manipulate their magnetic properties, for example, by using liquid/solid ion gating [8,14,15] or simply electrostatic doping [9,10]. One typical success is that, by using a liquid ion gate, the Curie temperature of a few layer Fe$_3$GeTe$_2$ can be tuned up to 300 K [8]. Looking for a new layered low-dimensional ferromagnetic material with intrinsic room-temperature T_C is extremely needed.

A recent theoretical calculation suggests that layered Cr$_x$Te$_y$ compounds have great potential as candidates for room-temperature two-dimensional ferromagnetic materials [16,17]. Cr$_x$Te$_y$ with various compositions have been synthesized including CrTe [18], Cr$_2$Te$_3$ [19,20], Cr$_3$Te$_4$ [21], and Cr$_5$Te$_8$ [22,23]; the phase diagrams have been reported by Chattopadhyay in detail [24]. In these compounds, there are alternating stacks of Cr-full and Cr-deficient layers along the c axis [25,26]. Cr content has been found to play an essential role in determining the crystal structure and magnetic properties. It is reported that Cr$_5$Te$_8$, Cr$_2$Te$_3$, and Cr$_3$Te$_4$ crystallize in monoclinic or trigonal structures, while Cr$_{1-x}$Te ($x < 0.1$) crystallizes in hexagonal NiAs-type structures [26]. The electronic band-structure calculations performed on CrTe, Cr$_2$Te$_3$, and Cr$_3$Te$_4$ suggest that Cr $3d_{z^2}$–Cr $3d_{z^2}$ along the crystallographic c direction overlaps strongly with the Cr $3d_{z^2}$–Cr $3d_{z^2}$ orbital at a relatively smaller nearest-neighbor Cr-Cr distance [25]. Critical behaviors have been studied extensively for layered-structure materials, such as Mn$_3$Si$_2$Te$_6$ [27], Cr$_2$Ge$_2$Te$_6$ [5,6], Cr$_2$Si$_2$Te$_6$ [28], Fe$_3$GeTe$_2$ [29], Cr$_5$Te$_8$ [30], and Cr$_{0.62}$Te [31]. The research of Cr$_5$Te$_8$ and Cr$_{0.62}$Te confirmed that long-range interaction of weak itinerant ferromagnetism persists in bulk with remarkable magnetocrystalline anisotropy. Anomalous Hall effect and topological Hall effect were observed in Cr$_{4.14}$Te$_8$ and Cr$_5$Te$_8$ [22,23,32]. With all the exotic properties discovered, Cr$_4$Te$_5$ has rarely been studied mainly due to the difficulty in precisely controlling the composition.

In this paper, high-quality single-crystalline Cr$_4$Te$_5$ was grown by chemical vapor transport method. The crystal structure, magnetic properties, magnetocaloric effect (MCE), and critical behavior were studied in detail. By comparing with the recently reported Cr$_5$Te$_8$, numerous distinctions have been
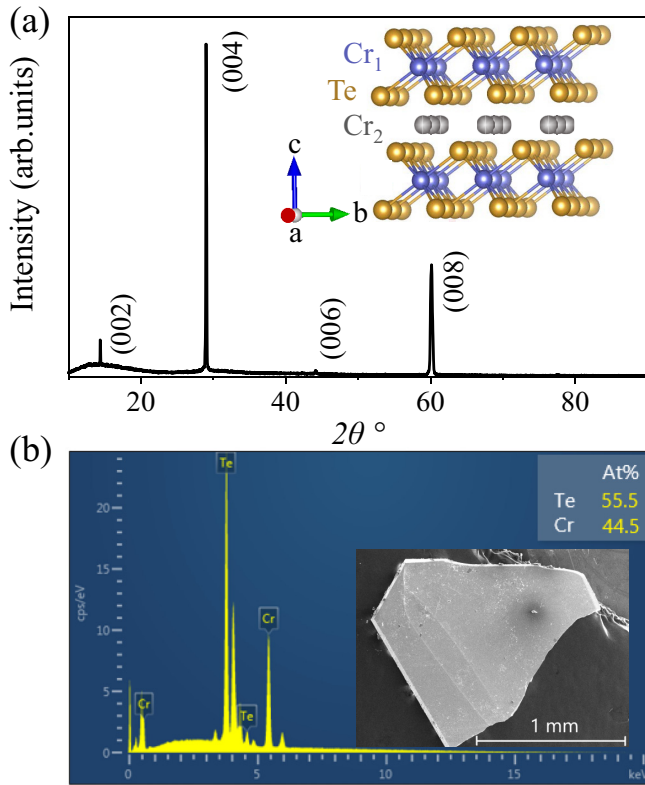
*junyi_ge@t.shu.edu.cn

FIG. 1. (a) The x-ray diffraction patterns of single crystalline Cr_4Te_5 showing $(00l)$ diffraction peaks. Schematic inset of Cr_4Te_5 crystal structure. Cr_1, Cr_2, and Te are denoted by blue, grey, and yellow balls, where Cr_1 and Cr_2 represent atoms in and between $CrTe_2$ layers, respectively. (b) The EDX of the crystal. The inset is the scanning electron microscope image of our studied sample.

FIG. 2. Temperature dependencies of magnetization curves after ZFC (solid) and FC (open) processes under various magnetic fields with H parallel to the (a) c axis and (b) ab plane, respectively. The inset in Fig. 2(a) is dM/dT vs T of the FC $M(T)$ curve for $H = 3000$ Oe. Isothermal magnetization loops of Cr_4Te_5 measured at $T = 2, 300, 350$, and 400 K for (c) $H \parallel c$ and (d) $H \parallel ab$.

discovered. The easy magnetization orientation turns from the c axis for Cr_5Te_8 to the ab plane for Cr_4Te_5, the RT magnetic entropy changes of Cr_4Te_5 show considerable potential in applications. Critical behavior analysis confirmed that Cr_4Te_5 belongs to second-order magnetic phase transition at T_C. By using the Kouvel-Fisher (KF) method, critical exponents were obtained: $\beta = 0.388$ with $T_C = 318.9$ K and $\gamma = 1.29$ with $T_C = 318.6$ K. The RT ferromagnetic phase transition and remarkable magnetocrystalline anisotropy of Cr_4Te_5 indicate its broad prospects in designing low-dimensional heterostructure and spintronic devices.

II. EXPERIMENTAL

Single-crystalline samples of Cr_4Te_5 were grown by the chemical vapor transport method [33]. Cr (99.99%; Alfa Aesar) and Te powders (99.99%; Alfa Aesar) were thoroughly mixed, and then sealed into a quartz tube with a partial pressure of argon. Iodine was used as the transport agent. The quartz tubes were heated to 400 °C in 4 h and kept at temperature for 10 h before further heating to 1000 °C on one side. At the same time, the other side of the quartz tube was heated to 820 °C. Single crystals with a layered structure and black metallic luster were observed at the cold side of the tube. The composition of the crystals was characterized with the energy dispersive x-ray spectroscopy (EDX). Single-
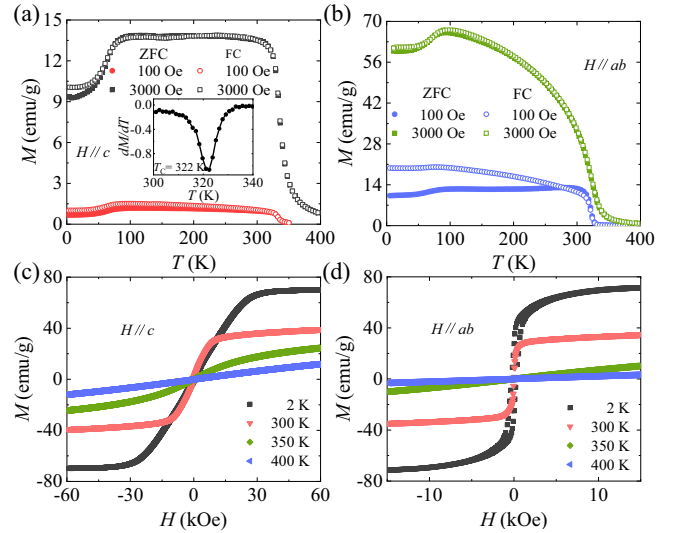
crystal compositions described in this paper all refer to the EDX values. The single crystal x-ray diffraction patterns were collected at room temperature with Cu K_α. The data of magnetization were measured by using a Quantum Design Physical Property Measurement System (PPMS-14T) with a vibrating sample magnetometer option.

III. RESULTS AND DISCUSSIONS

In Fig. 1(a), sharp Bragg peaks are observed in the XRD pattern, which can be indexed as the $(00l)$, suggesting that the c axis is perpendicular to the slab surface of crystal [30,31]. No extra peak is observed within the resolution of our instrument, indicating the high quality of our sample. We also noticed that the $(00l)$ peaks move to lower 2θ values compared with other Cr_5Te_8 compounds [30,31], which indicates more Cr atoms intercalate into $CrTe_2$ layers and leads to an increase of the lattice parameter. The inset of Fig. 1(a) shows the crystal structure of Cr_4Te_5, where Cr and Te atoms form the corner-sharing octahedral with the intercalation of Cr atoms between the $CrTe_2$ layers. The EDX data in Fig. 1(b) confirms the stoichiometry of Cr_4Te_5. The as-grown single crystals are in a platelike form with metallic luster, as illustrated in the inset of Fig. 1(b).

To explore the magnetic properties, the temperature dependence of magnetization measurements along both the ab plane and c axis have been performed under various magnetic fields and in a large temperature range. Figures 2(a) and 2(b) show the temperature-dependent magnetization of Cr_4Te_5 measured under $H = 100$ Oe, 3000 Oe with the field direction parallel to the c axis and ab plane, respectively. The paramagnetic (PM) to FM transition occurs in both zero-field-cooling (ZFC) and field-cooling (FC) processes. At around 320 K and $H = 100$ Oe, the magnetization observed in ZFC curves diverge from
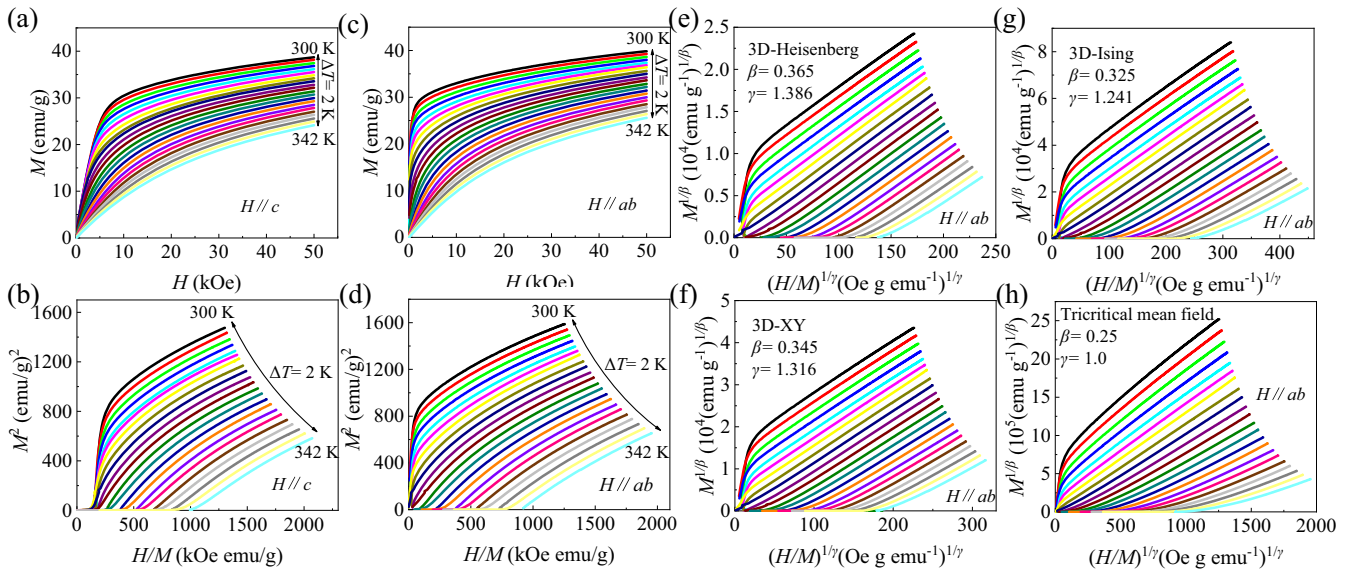
FIG. 3. The initial isothermal magnetization curves measured along the (a) c axis and (b) ab plane around T_C for Cr_4Te_5. Arrott plots of M^2 vs H/M along the (c) c axis and (d) ab plane. The modified Arrott plots of $M^{1/\beta}$ vs $(H/M)^{1/\gamma}$ with parameters of (e) 3D-Heisenberg model, (f) 3D-XY model, (g) 3D-Ising model, and (h) tricritical mean-field model. The straight lines are the linear fits of isotherms at different temperatures. Figures 3(e)–3(h) are derived from the isothermal magnetization curves with $H \parallel ab$.

that of the FC curve. Similar behavior was also reported in Cr_5Te_8, which can be ascribed to the appearance of a canted antiferromagnetic (AFM) structure [34]. However, for Cr_5Te_8, the deviation appears at a temperature much below T_C, while for Cr_4Te_5, it occurs at relatively high temperature close to T_C. This result indicates that higher Cr content raises the deviation temperature of the ZFC and FC curves, at which canted-AFM occurs. Moreover, the high applied field suppresses the canted-AFM phase to lower ,s as can be observed in Figs. 2(a) and 2(b). The obvious decrease of magnetization at 96 K for both ZFC and FC curves can be attributed to a transition from the FM to AFM phase. The Curie temperature $T_C = 322$ K is estimated from the minimum value of the dM/dT-T curve as shown in the inset of Fig. 2(a). The observed small coercive forces (H_C) at $T = 2$ K ($H_C = 552$ Oe for $H \parallel c$ and 278 Oe for $H \parallel ab$) suggest a soft ferromagnetic nature of Cr_4Te_5.

For the previous reported Cr_xTe_y compounds, such as $Cr_{4.14}Te_8$ [32], Cr_5Te_8 [35], and Cr_3Te_4 [36], the c axis is the easy magnetization axis while along ab-plane the magnetization is hard to saturate. However, our Cr_4Te_5 crystal displays an opposite behavior, as shown in Figs. 2(c) and 2(d), where $M(H \parallel ab)$ and $M(H \parallel c)$ saturate at 10 kOe and 30 kOe, respectively. The saturation moment at $T = 2K$ is $M_s \approx 2.64$ μ_B/Cr with $H \parallel c$; this value is larger than the reported $M_s \approx 1.57$ μ_B/Cr for Cr_5Te_8 [35], the expected value for the Cr-free ion is $3\mu_B$/Cr, due to the presence of the itinerancy nature of the d electrons in Cr-Te compounds [37,38]. Our relatively large M_s can be ascribed to the increase of Cr content in $CrTe_2$ layers, leading to stronger itinerancy. For the Cr-Te systems, there also exists strong hybridization between the Cr $3d$ band and the Te $5p$ bands. The electron-correlation effect and the interlayer coupling plays an important role in the magnetic interactions [20,37,38]. We suggest that the high Curie temperature can be attributed to the large amount of Cr atoms intercalated into $CrTe_2$ layers, where the local

spins of intercalated Cr ions align ferromagnetically through the Te $5p$. This indirect exchange interaction raises the Curie temperature. In the meantime, FM coupling in the ab plane has also been enhanced. As a result, the easy magnetization orientation is transformed from the c axis into the ab plane.

To further understand the nature of the FM transition in Cr_4Te_5 and investigate the MCE, the isothermal magnetization is measured around the Curie temperature to investigate the critical exponents associated with the phase transition in detail. Initial isothermal magnetization $M(H)$ around T_C was measured from $T = 300$ K to $T = 342$ K at an interval of 2 K along the c axis [Fig. 3(a)] and ab plane [Fig. 3(c)]. Figures 3(b) and 3(d) present the Arrott plot of M^2 vs H/M [39]. In Figs. 3(b) and 3(d), the curves are not parallel at the high-field region, suggesting that the mean-field theory is not suitable for Cr_4Te_5. This is reasonable, considering that the Coulomb correlation and spin fluctuations are significant in an itinerant ferromagnet [40], while the mean-field theory neglects its impact. According to the Banerjee criterion [41], the positive slopes of M^2 vs H/M curves in the vicinity of the phase-transition temperature confirms a second-order phase transitions in Cr_4Te_5.

Since the traditional Arrott plot cannot explain the magnetic interaction in Cr_4Te_5 appropriately, a modified Arrott plots (MAP) is often used, based on four typical models: (1) the 3D-Heisenberg model ($\beta = 0.365$, $\gamma = 1.386$) [42], (2) the 3D-XY model ($\beta = 0.345$, $\gamma = 1.316$) [43], (3) the 3D-Ising model ($\beta = 0.325$, $\gamma = 1.241$) [42], (4) the tricritical mean-field model ($\beta = 0.25$, $\gamma = 1$) [44]. The results are shown in Figs. 3(e)–3(h), where the observed curves are not greatly parallel. This suggests that the above-mentioned four models are not applicable in Cr_4Te_5.

For the purpose of obtaining more accurate critical exponents and the critical temperature, a rigorous iterative approach has been adopted [45]. In the modified Arrott plot, the
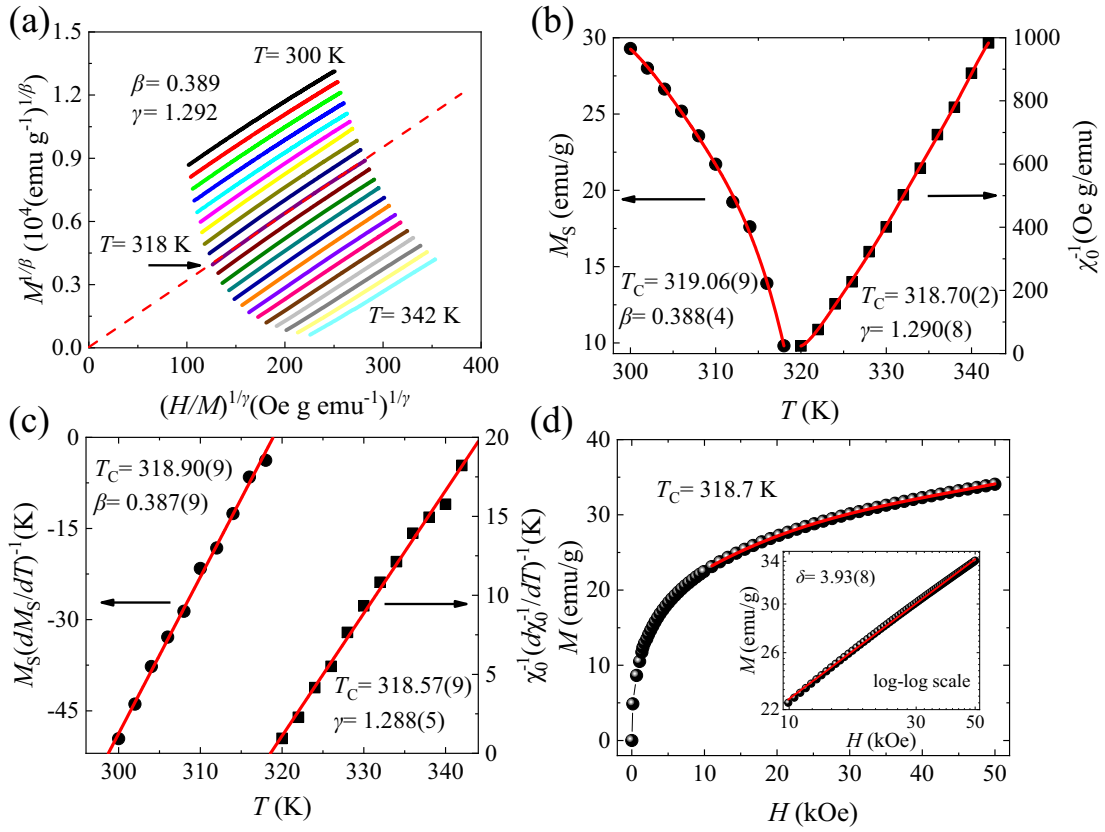
FIG. 4. (a) Modified Arrott plot of $M^{1/\beta}$ vs $(H/M)^{1/\gamma}$ at high field values with the parameters of $\beta = 0.389$ and $\gamma = 1.292$ with a red linear fitting dashed curve. (b) Temperature-dependent spontaneous magnetization M_S (left) and the inverse initial susceptibility χ^{-1} (right) for Cr_4Te_5. The red solid curves fit with Eqs. (1) and (2) with the fitting parameters indicated. (c) Kouvel-Fisher plot showing the temperature dependencies of $M_S(T)/[dM_S(T)/dT]$ (circles) and $\chi_0^{-1}(T)/[d\chi_0^{-1}(T)/dT]$ (squares) for Cr_4Te_5. The red solid lines are fitting by Eqs. (4) and (5). (d) The isotherm M vs H plot measured at $T_C = 318.7$ K with a red solid line fitting by Eqs. (3) for Cr_4Te_5. Inset: The corresponding log-log scale.

linear extrapolations of the modified curves from the high-field region to the axis $M^{1/\beta}$ and $(H/M)^{1/\gamma}$ yield reliable values of $M_S(T)$ and $\chi^{-1}(T)$, respectively. The obtained $M_S(T)$ and $\chi^{-1}(T)$ parameters can be used to fit a new set of β and γ by following Eqs. (1) and (2), where $\varepsilon = (T-T_C)/T_C$, M_0, h_0/m_0, and D are the critical amplitudes [46,47].

$$M_s(T) = M_0(-\varepsilon)^\beta, \quad \varepsilon < 0, \quad T < T_C, \tag{1}$$

$$\chi_0^{-1}(T) = (h_0/m_0)\varepsilon^\gamma, \quad \varepsilon > 0, \quad T > T_C, \tag{2}$$

$$M = DH^{1/\delta}, \quad \varepsilon = 0, \quad T = T_C, \tag{3}$$

Then, the fitted exponents can be used to reconstruct a modified Arrott plot. This procedure is repeated until the values of β and γ are convergent. It's worth noting that the exponents obtained by this approach are independent of the initial parameters, which implies the reliability of these critical exponents. As shown in Fig. 4(a), a set of parallel straight lines at high fields ($H > 13$ kOe) are achieved by proper selection of β and γ values. The red dotted line is a linear fitting of isothermal magnetization curve at $T = 318$ K. This curve almost extrapolates to the (0,0) point in Fig. 4(a), indicating the Curie temperature is close to 318 K. By using Eqs. (1) and (2), the final obtained values

$\beta = 0.388(4)$, with $T_C = 319.06(9)$ K, and $\gamma = 1.290(8)$, with $T_C = 318.70(2)$ K, are presented in Fig. 4(b). To obtain more accurate critical exponents of Cr_4Te_5, KF method [48] is used, as illustrated in Fig. 4(c).

$$\frac{M_s(T)}{dM_s(T)/dT} = \frac{T - T_C}{\beta}, \tag{4}$$

$$\frac{\chi_0^{-1}(T)}{d\chi_0^{-1}(T)/dT} = \frac{T - T_C}{\gamma}, \tag{5}$$

According to this method, the linear functions in the region below and above T_C yield $\beta = 0.387(9)$ with $T_C = 318.90(9)$ K, and $\gamma = 1.288(5)$ with $T_C = 318.57(9)$ K, respectively. The values of β, γ, and T_C from the KF method are consistent with those generated from the iterative MAP, which further confirms that the critical values are reliable and intrinsic.

Accordingly, following the Widom scaling relation [49],

$$\delta = 1 + \frac{\gamma}{\beta}, \tag{6}$$

the critical exponents $\delta = 4.32(3)$ and $\delta = 4.32(2)$ are derived from MAP and KF methods, respectively. δ can also be obtained directly by the isothermal magnetization $M(H)$ at T_C as shown in the inset of Fig. 4(d), using the log-log scale plot
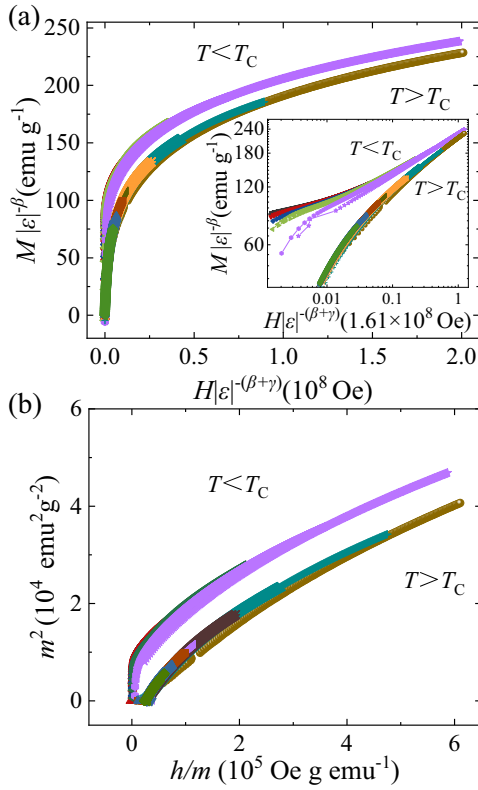
FIG. 5. (a) The plots of normalized magnetization m as a function of renormalized field h below and above T_C for Cr_4Te_5. Inset: The same plot in log-log scale. (b) Normalized magnetization m^2 as a function of h/m for Cr_4Te_5.

with a fitting curve. Following Eqs. (3), the log(M)-log(H) relation yields straight line at higher field range (H > 10 kOe) with the slope $1/\delta$, where $\delta = 3.93(8)$ is obtained. The value of δ obtained by critical isothermal analysis is very close to the result from the Widom scaling law with a slight deviation indicating that the critical behavior of Cr_4Te_5 may have complex competition among several magnetic interactions, e.g., AFM, FM, and PM. Therefore, all the critical exponents β, γ, δ, and T_C obtained in our study are self-consistent and reasonably accurate within the experimental precision.

The reliability of the obtained critical exponents and critical temperature has been verified by scaling analysis. For magnetic systems in their critical asymptotic region, the scaling equation of state can be expressed as [46]

$$M(H, \varepsilon) = \varepsilon^\beta f_\pm(H/\varepsilon^{\beta+\gamma}), \tag{7}$$

where $f\pm$ are the regular functions defined as f_+ for $\varepsilon > 0$ and f_- for $\varepsilon < 0$, respectively. Equation (7) can also be written as

$$m = f_\pm(h), \tag{8}$$

where $m \equiv \varepsilon^{-\beta}M(H, \varepsilon)$ is the renormalized magnetization and $h \equiv \varepsilon^{-(\beta+\gamma)}H$ is the renormalized field. Such a scaling hypothesis implies that, if the β, γ, and δ values are appropriately chosen, the scaled m and h should fall on two universal curves: one for $\varepsilon > 0$ and the other for $\varepsilon < 0$. According to Eq. (8), the scaled m vs h curves are plotted in Fig. 5(a). Obvi-

ously, the lines are separated into two branches, which is more visible in the logarithmic scale shown in the inset of Fig. 5(a). This can be further verified by a more rigorous method using an m^2 vs h/m plot [42], as shown in Fig. 5(b), in which all the curves also collapse into two divided branches. The well-rescaled curves further ensure that the obtained critical exponents and T_C are reliable and accordant with the scaling hypothesis.

The obtained critical exponents, as well as those calculated from different theoretical models [42–44] and related Cr-Te materials [30,31], are summarized in Table I for comparison. It seems that the obtained exponents of Cr_4Te_5 cannot be categorized into any single conventional universality class. The exponent β lies between the 3D-Heisenberg model and the mean-field model but closer to the former, which indicates the exchange interaction in Cr_4Te_5 is possible to be a long-range type. However, γ is near the 3D-Ising model and the 3D-XY model, which could be attributed to the apparent magnetocrystalline anisotropy in the ground state of Cr_4Te_5. Besides, it is critical to analyze the nature and the range of interaction in Cr_4Te_5. It is known that the universality class of magnetic phase transition depends on the range of the exchange interaction J(r). Based on renormalization-group theory analysis, the interaction decays with a distance r as $J(r) \sim e^{-r/b}$ for short-range exchange, and $J(r) \sim r^{-(d+\sigma)}$ for long-range exchange, where r is the distance, b is the spatial scaling factor, d is the spatial dimension of the system, and σ is the range of exchange interaction [50,51]. The relationship between σ and critical exponent γ can be determined as follows [50]:

$$\gamma = 1 + \frac{4}{d}\left(\frac{n+2}{n+8}\right)\Delta\sigma + \frac{8(n+2)(n-4)}{d^2(n+8)^2}$$
$$\times \left[1 + \frac{2G\left(\frac{d}{2}\right)(7n+20)}{(n-4)(n+8)}\right]\Delta\sigma^2, \tag{9}$$

where $\Delta\sigma = \sigma - \frac{d}{2}$, $G\left(\frac{d}{2}\right) = 3 - \frac{1}{4}\left(\frac{d}{2}\right)^2$ and n is the spin dimensionality. The renormalization group theory analysis also suggests that the range of the spin interaction is short or long depending on $\sigma > 2$ or $\sigma < 2$, respectively. For Cr_4Te_5, to obtain σ, d, and n in this system, a process similar to Ref. [51] have been followed, where the parameter σ in Eq. (9) is adjusted for specific values of $\{d : n\}$ so it gives a value for γ close to the experimentally obtained $\gamma = 1.288(5)$. The obtained value σ is then used to calculate the other exponents by the following expressions: $\nu = \gamma/\sigma$, $\alpha = 2 - \nu d$, $\beta = (2 - \alpha - \gamma)/2$, and $\sigma = 1 + \gamma/\beta$, where ν and α are the critical exponents of correlation length. This procedure is repeated for different sets of $\{d : n\}$. It is found that for Cr_4Te_5 close to the 3D-Heisenberg-like type $\{d = 3, n = 3\}$ and $\sigma = 1.85$ with long-range spin interaction, the interaction decays with distance as $J(r) \approx r^{-4.85}$. Because of its evident strong magnetocrystalline anisotropy, long-range magnetic interaction for the bulk, and layered structure, Cr_4Te_5 has the potential to maintain its long-range magnetic coupling down to the 2D limit and design Van der Waals heterostructure.

RT ferromagnetism persisting in Cr_4Te_5 stimulated us to study the MCE of this material by using the Maxwell relation [52]; the isothermal magnetic entropy change $\Delta S_M(T, H)$ is

TABLE I. Comparison of critical exponents of Cr_4Te_5 with related Cr_xTe_y samples and different theoretical models.

Composition	Reference	Technique	β	γ	δ	J(r)
Cr_4Te_5	This paper	MAP	0.388(4)	1.290(8)	4.32(3)	
	This paper	KF method	0.387(9)	1.288(5)	4.32(2)	$r^{-4.85}$
	This paper	Critical isotherm			3.93(8)	
Theory	[39]	Mean-field	0.5	1.0	3	
Theory	[42]	3D-Heisenberg	0.365	1.386	4.80	
Theory	[42]	3D-Ising	0.325	1.241	4.82	
Theory	[43]	3D-XY	0.345	1.361	4.81	
Theory	[44]	Tricritical mean field	0.25	1.0	5	
Cr_5Te_8	[30]	KF method	0.321(7)	1.27(2)	4.9(2)	$r^{-4.94}$
$Cr_{0.62}Te$	[31]	KF method	0.315(7)	1.81(2)	6.35(4)	$r^{-4.626}$

presented below:

$$\Delta S_M(T, H) = \int_0^H \left(\frac{\partial S}{\partial H}\right)_T dH = \int_0^H \left(\frac{\partial M}{\partial T}\right)_H dH. \quad (10)$$

Considering the magnetization measured at small temperature intervals and discrete fields, $\Delta S_M(T_i, H)$ can be expressed as [53]

$$\Delta S_M(T_i, H) = \frac{\int_0^H M(T_i, H)dH - \int_0^H M(T_{i+1}, H)dH}{T_i - T_{i+1}}. \quad (11)$$

Derived on isothermal $M(H)$ curves, Figs. 6(a) and 6(b) show $-\Delta S_M$ versus temperature in various applied fields with $H \parallel c$ and $H \parallel ab$, respectively. As expected for $-\Delta S_M$, both (a) and (b) exhibit a broad bump in the vicinity of T_C where magnetic entropy changes dramatically. Besides, all values of $-\Delta S_M$ in Figs. 6(a) and 6(b) are negative—this is a characteristic of the MCE at a second-order PM-FM phase transition. Furthermore, for both $H \parallel c$ and $H \parallel ab$, the maximum of ΔS_M increases linearly with applied field as shown in Figs. 6(a) and 6(b). The maximum magnetic entropy change of $-\Delta S_M$ is about 2.42 J kg^{-1} K^{-1} with $H \parallel c$ and 2.58 J kg^{-1}K^{-1} with $H \parallel ab$. This value is slightly larger than 2.38 J kg^{-1}K^{-1} for monoclinic Cr_5Te_8 [30], but quite larger than trigonal Cr_5Te_8 [54] with 1.93 J kg^{-1} K^{-1}

for $H \parallel c$ at applied field of 50 kOe. The large value of Cr_4Te_5 may originate from the stronger FM coupling along both the c axis and ab plane, which can be explained by the enhancement of itinerancy as we mentioned above. Besides, by comparing MCE of Cr_4Te_5 and Cr_5Te_8 [54], an interesting phenomenon is observed. For Cr_5Te_8 with $H = 50$ kOe, the maximum value of $-\Delta S_M$ is observed with the magnetic field along the easy magnetization orientation (c axis), while for Cr_4Te_5, the maximum value of $-\Delta S_M$ is observed with field parallel to the ab plane. This result is also consistent with previous research [36] that, by increasing Chromium content, FM coupling is enhanced in both the c axis and ab plane, and even reaches a maximum value as ultimately shown in Figs. 2(c) and 2(d).

IV. CONCLUSIONS

In summary, the Cr_4Te_5 single crystal has been successfully grown by chemical vapor transport method. The magnetic properties, MCE, and critical behavior have been investigated in detail. The RT ferromagnetism and broad range of magnetic entropy change temperature of Cr_4Te_5 show its considerable potential in the application of magnetic refrigerant materials. Moreover, according to the study of critical phenomenon at the FM-PM phase transition, the
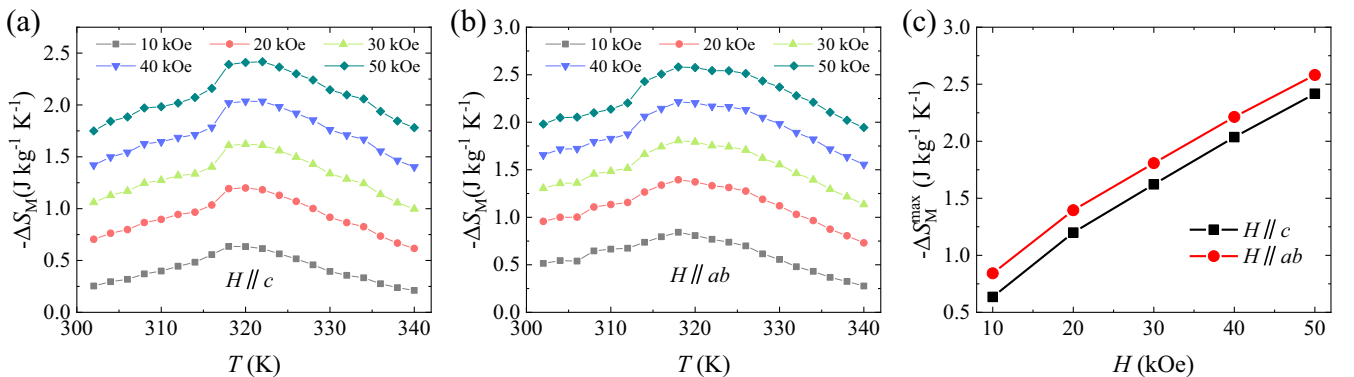

FIG. 6. Magnetic entropy change $-\Delta S_M$ versus temperature at various magnetic fields for (a) $H \parallel c$ and (b) $H \parallel ab$. (c) Maximum entropy change $-\Delta S_M^{max}$ as a function of field for $H \parallel c$ and $H \parallel ab$.

critical exponents β, γ, and σ are estimated from various approaches. The obtained critical exponents are very close to the 3D-Heisenberg model with $\{d : n\} = \{3 : 3\}$. Long-range interaction has been classified based on the observed value $\sigma = 1.89$, which decays as $J(r) \approx r^{-4.85}$. By exfoliating bulk Cr_4Te_5 to monolayer, novel phenomena and mechanisms are expected for next-step research.

[1] A. K. Geim, Science. **324**, 1530 (2009).

[2] D. Zhong, K. L. Seyler, X. Yu, L. Peng, R. Cheng. N. Sivadas, B. Huang, E. Schmidgall, T. Taniguchi, K. Watanabe, M. A. McGuire, W. Yao, D. Xiao, K. M. C. Fu, and X. D. Xu, Sci. Adv. **3**, e1603113 (2017).

[3] A. K. Geim and I. V. Grigorieva, Nature. **499**, 419 (2013).

[4] J. T. Heron, M. Trassin, K. Ashraf, M. Gajek, Q. He, S. Y. Yang, D. E. Nikonov, Y.-H. Chu, S. Salahuddin, and R. Ramesh, Phys. Rev. Lett. **107**, 217202 (2011).

[5] Y. Liu and C. Petrovic, Phys. Rev. B **96**, 054406 (2017).

[6] W. Liu, Y. Dai, Yu.-E. Yang, J. Fan, L. Pi, L. Zhang, and Y. Zhang, Phys. Rev. B **98**, 214420 (2018).

[7] T. J. Williams, A. A. Aczel, M. D. Lumsden, S. E. Nagler, M. B. Stone, J.-Q. Yan, and D. Mandrus, Phys. Rev. B **92**, 144404 (2015).

[8] Y. J. Deng, Y. J. Yu, Y. C. Song, J. Z. Zhang, N. Z. Wang, Z. Y. Sun, Y. F. Yi, Y. Z. Wu, S. W. Wu, J. Y. Zhu, J. Wang, and X. H. Chen, and Y. B. Zhang, Nature **563**, 94 (2018).

[9] S. W. Jiang, L. Z. Li, Z. F. Wang, K. F. Mak, and J. Shan, Nat. Nanotechnol. **13**, 549 (2018).

[10] S. W. Jiang, J. Shan, and K. F. Mak, Nat Mater. **17**, 406 (2018).

[11] B. Huang, G. Clark, D. R. Klein, D. MacNeill, E. Navarro-Moratalla, K. L. Seyler, N. Wilson, M. A. McGuire, D. H. Cobden, D. Xiao, W. Yao, P. Jarillo-Herrero, and Xiaodong Xu, Nat. Nanotechnol. **13**, 544 (2018).

[12] N. D. Mermin and H. Wagner, Phys. Rev. Lett. **17**, 1133 (1966).

[13] B. Huang, G. Clark, E. Navarro-Moratalla, D. R. Klein, R. Cheng, K. L. Seyler, D. Zhong, E. Schmidgall, M. A. McGuire, D. H. Cobden, W. Yao, D. Xiao, P. Jarillo-Herrero, and X. Xu, Nature. **546**, 270 (2017).

[14] F. Matsukura, Y. Tokura, and H. Ohno, Nat. Nanotechnol. **10**, 209 (2015).

[15] M. Weisheit, S. Fähler, A. Marty, Y. Souche, C. Poinsignon, and D. Givord, Science **315**, 349 (2007).

[16] X. W. Zhang, B. Wang, Y. L. Guo, Y. H. Zhang, Y. F. Chen, and Z. L. Wang, Nanoscale Horiz. **4**, 859 (2019).

[17] Y. Zhu, X. H. Kong, T. D. Rhone, and H. Guo, Phys. Rev. Mater. **2**, 081001 (2018).

[18] T. Eto, M. Ishizuka, S. Endo, T. Kanomata, and T. Kikegawa, J. Alloy. Compd. **315**, 16 (2001).

[19] F. Wang, J. Du, F. Sun, R. F. Sabirianov, N. Al-Aqtash, D. Sengupta, H. Zeng, and X. H. Xu, Nanoscale. **10**, 11028 (2018).

[20] T. Hamasaki, T. Hashimoto, Y. Yamaguchi, and H. Watanabe, Solid State Commun. **16**, 895 (1975).

[21] B. Hessen, T. Siegrist, T. Palstra, S. M. Tanzler, and M. L. Steigerwald, Inorg. Chem. **32**, 5165 (1993).

[22] Y. H. Wang, J. Yan, J. B. Li, S. S. Wang, M. Song, J. P. Song, Z. H. Li, K. Chen, Y. L. Qin, L. S. Ling, H. F. Du, L. Cao, X. Luo, Y. M. Xiong, and Y. P. Sun, Phys. Rev. B **100**, 024434 (2019).

[23] Y. Liu and C. Petrovic, Phys. Rev. B **98**, 195122 (2018).

[24] G. Chattopadhyay, J. Phase Equilib. **15**, 431 (1994).

[25] J. Dijkstra, H. H. Weitgering, C. F. van Bruggen, C. Haas, and R. A. de Groot, J. Phys. Condens. Matter. **1**, 9141 (1989).

[26] H. Ipser, K. L. Komarek, and K. O. Klepp, J. Less Common Metals **92**, 265 (1983).

[27] Y. Liu and C. Petrovic, Phys. Rev. B **98**, 064423 (2018).

[28] B. J. Liu, Y. M. Zou, L. Zhang, S. M. Zhou, Z. Wang, W. K. Wang, Z. Qu, and Y. H. Zhang, Sci. Rep. **6**, 33873 (2016).

[29] Y. Liu, V. N. Ivanovski, and C. Petrovic, Phys. Rev. B **96**, 144429 (2017).

[30] X. Zhang, T. L. Yu, Q. Y. Xue, M. Lei, and R. Z. Jiao, J. Alloy. Compd. **750**, 798 (2018).

[31] Y. Liu and C. Petrovic, Phys. Rev. B **96**, 134410 (2017).

[32] Y. Yan, X. Luo, G. T. Lin, F. C. Chen, J. J. Gao, Y. Sun, L. Hu, P. Tong, W. H. Song, S. Z. Gao, W. J. Lu, X. B. Zhu, and Y. P. Sun, Europhys. Lett. **124**, 67005 (2018).

[33] M. Yamaguchi and T. Hashimoto, J. Phys. Soc. Jpn. **32**, 635 (1972).

[34] Z. L. Huang, W. Kockelmann, M. Telling, and W. Bensch, Solid State Sci. **10**, 1099 (2008).

[35] R. Mondal, R. Kulkarni, and A. Thamizhavel, J. Magn. Magn. Mater. **483**, 27 (2019).

[36] L.-Z. Zhang, X.-D. He, A.-L. Zhang, Q.-L. Xiao, W.-L. Lu, F. Chen, Z. Feng, S. Cao, J. Zhang, and J.-Y. Ge, APL Mater. **8**, 031101 (2020).

[37] A. F. Anderson, Acta. Chem. Scand. **24**, 3495 (1970).

[38] K. Shimada, T. Saitoh, H. Namatame, A. Fujimori, S. Ishida, S. Asano, and M. Matoba, and S. Anzai, Phys. Rev. B **53**, 7673 (1996).

[39] A. Arrott, Phys. Rev. **108**, 1394 (1957).

[40] T. N. Lamichhane, L. Xiang, Q. Lin, T. Pandey, D. S. Parker, T.-H. Kim, L. Zhou, M. J. Kramer, S. L. Bud'ko, and P. C. Canfield, Phys. Rev. Mater. **2**, 084408 (2018).

[41] B. K. Banerjee, Phys. Lett. **12**, 16 (1964).

[42] S. N. Kaul, J. Magn. Magn. Mater. **53**, 5 (1985).

[43] J. C. Le Guillou and J. Zinn-Justin, Phys. Rev. B **21**, 3976 (1980).

[44] D. Kim, B. Revaz, B. L. Zink, F. Hellman, J. J. Rhyne, and J. F. Mitchell, Phys. Rev. Lett. **89**, 227202 (2002).

[45] A. K. Pramanik and A. Banerjee, Phys. Rev. B **79**, 214426 (2009).

[46] H. E. Stanley, *Introduction to Phase Transitions and Critical Phenomena* (Oxford University Press, London, 1971).

[47] M. E. Fisher, Rep. Prog. Phys. **30**, 615 (1967).

[48] J. S. Kouvel and M. E. Fisher, Phys. Rev. **136**, A1626 (1964).

[49] B. Widom, J. Chem. Phys. **43**, 3898 (1965).

[50] M. E. Fisher, S.-k. Ma, and B. Nickel, Phys. Rev. Lett. **29**, 917 (1972).

[51] S. F. Fischer, S. N. Kaul, and H. Kronmuller, Phys. Rev. B **65**, 064443 (2002).

[52] J. Amaral, M. Reis, V. Amaral, T. Mendonc, J. Araujo, M. Sa, P. Tavares, and J. Vieira, J. Magn. Magn. Mater. **290**, 686 (2005).

[53] M. H. Phan and S. C. Yu, J. Magn. Magn. Mater. **308**, 325 (2007).

[54] X.-H. Luo, W.-J. Ren, and Z.-D. Zhang, J. Magn. Magn. Mater. **445**, 37 (2018).